

Proceedings of the 12th International Conference on
Computational Fluid Dynamics in the Oil & Gas,
Metallurgical and Process Industries

Progress in Applied CFD – CFD2017



SINTEF Proceedings

Editors:

Jan Erik Olsen and Stein Tore Johansen

Progress in Applied CFD – CFD2017

Proceedings of the 12th International Conference on Computational Fluid Dynamics
in the Oil & Gas, Metallurgical and Process Industries

SINTEF Academic Press

SINTEF Proceedings no 2

Editors: Jan Erik Olsen and Stein Tore Johansen

Progress in Applied CFD – CFD2017

Selected papers from 10th International Conference on Computational Fluid Dynamics in the Oil & Gas, Metallurgical and Process Industries

Key words:

CFD, Flow, Modelling

Cover, illustration: Arun Kamath

ISSN 2387-4295 (online)

ISBN 978-82-536-1544-8 (pdf)

© Copyright SINTEF Academic Press 2017

The material in this publication is covered by the provisions of the Norwegian Copyright Act. Without any special agreement with SINTEF Academic Press, any copying and making available of the material is only allowed to the extent that this is permitted by law or allowed through an agreement with Kopinor, the Reproduction Rights Organisation for Norway. Any use contrary to legislation or an agreement may lead to a liability for damages and confiscation, and may be punished by fines or imprisonment

SINTEF Academic Press

Address: Forskningsveien 3 B
 PO Box 124 Blindern
 N-0314 OSLO

Tel: +47 73 59 30 00

Fax: +47 22 96 55 08

www.sintef.no/byggforsk

www.sintefbok.no

SINTEF Proceedings

SINTEF Proceedings is a serial publication for peer-reviewed conference proceedings on a variety of scientific topics.

The processes of peer-reviewing of papers published in SINTEF Proceedings are administered by the conference organizers and proceedings editors. Detailed procedures will vary according to custom and practice in each scientific community.

PREFACE

This book contains all manuscripts approved by the reviewers and the organizing committee of the 12th International Conference on Computational Fluid Dynamics in the Oil & Gas, Metallurgical and Process Industries. The conference was hosted by SINTEF in Trondheim in May/June 2017 and is also known as CFD2017 for short. The conference series was initiated by CSIRO and Phil Schwarz in 1997. So far the conference has been alternating between CSIRO in Melbourne and SINTEF in Trondheim. The conferences focuses on the application of CFD in the oil and gas industries, metal production, mineral processing, power generation, chemicals and other process industries. In addition pragmatic modelling concepts and bio-mechanical applications have become an important part of the conference. The papers in this book demonstrate the current progress in applied CFD.

The conference papers undergo a review process involving two experts. Only papers accepted by the reviewers are included in the proceedings. 108 contributions were presented at the conference together with six keynote presentations. A majority of these contributions are presented by their manuscript in this collection (a few were granted to present without an accompanying manuscript).

The organizing committee would like to thank everyone who has helped with review of manuscripts, all those who helped to promote the conference and all authors who have submitted scientific contributions. We are also grateful for the support from the conference sponsors: ANSYS, SFI Metal Production and NanoSim.

Stein Tore Johansen & Jan Erik Olsen



Organizing committee:

Conference chairman: Prof. Stein Tore Johansen

Conference coordinator: Dr. Jan Erik Olsen

Dr. Bernhard Müller

Dr. Sigrid Karstad Dahl

Dr. Shahriar Amini

Dr. Ernst Meese

Dr. Josip Zoric

Dr. Jannike Solsvik

Dr. Peter Witt

Scientific committee:

Stein Tore Johansen, SINTEF/NTNU

Bernhard Müller, NTNU

Phil Schwarz, CSIRO

Akio Tomiyama, Kobe University

Hans Kuipers, Eindhoven University of Technology

Jinghai Li, Chinese Academy of Science

Markus Braun, Ansys

Simon Lo, CD-adapco

Patrick Segers, Universiteit Gent

Jiyuan Tu, RMIT

Jos Derksen, University of Aberdeen

Dmitry Eskin, Schlumberger-Doll Research

Pär Jönsson, KTH

Stefan Pirker, Johannes Kepler University

Josip Zoric, SINTEF

CONTENTS

PRAGMATIC MODELLING	9
On pragmatism in industrial modeling. Part III: Application to operational drilling	11
CFD modeling of dynamic emulsion stability	23
Modelling of interaction between turbines and terrain wakes using pragmatic approach	29
FLUIDIZED BED	37
Simulation of chemical looping combustion process in a double looping fluidized bed reactor with cu-based oxygen carriers.....	39
Extremely fast simulations of heat transfer in fluidized beds.....	47
Mass transfer phenomena in fluidized beds with horizontally immersed membranes	53
A Two-Fluid model study of hydrogen production via water gas shift in fluidized bed membrane reactors	63
Effect of lift force on dense gas-fluidized beds of non-spherical particles	71
Experimental and numerical investigation of a bubbling dense gas-solid fluidized bed	81
Direct numerical simulation of the effective drag in gas-liquid-solid systems	89
A Lagrangian-Eulerian hybrid model for the simulation of direct reduction of iron ore in fluidized beds.....	97
High temperature fluidization - influence of inter-particle forces on fluidization behavior	107
Verification of filtered two fluid models for reactive gas-solid flows	115
BIOMECHANICS.....	123
A computational framework involving CFD and data mining tools for analyzing disease in carotid artery	125
Investigating the numerical parameter space for a stenosed patient-specific internal carotid artery model.....	133
Velocity profiles in a 2D model of the left ventricular outflow tract, pathological case study using PIV and CFD modeling.....	139
Oscillatory flow and mass transport in a coronary artery.....	147
Patient specific numerical simulation of flow in the human upper airways for assessing the effect of nasal surgery.....	153
CFD simulations of turbulent flow in the human upper airways	163
OIL & GAS APPLICATIONS	169
Estimation of flow rates and parameters in two-phase stratified and slug flow by an ensemble Kalman filter	171
Direct numerical simulation of proppant transport in a narrow channel for hydraulic fracturing application	179
Multiphase direct numerical simulations (DNS) of oil-water flows through homogeneous porous rocks	185
CFD erosion modelling of blind tees	191
Shape factors inclusion in a one-dimensional, transient two-fluid model for stratified and slug flow simulations in pipes	201
Gas-liquid two-phase flow behavior in terrain-inclined pipelines for wet natural gas transportation	207

NUMERICS, METHODS & CODE DEVELOPMENT	213
Innovative computing for industrially-relevant multiphase flows	215
Development of GPU parallel multiphase flow solver for turbulent slurry flows in cyclone.....	223
Immersed boundary method for the compressible Navier–Stokes equations using high order summation-by-parts difference operators	233
Direct numerical simulation of coupled heat and mass transfer in fluid-solid systems	243
A simulation concept for generic simulation of multi-material flow, using staggered Cartesian grids.....	253
A cartesian cut-cell method, based on formal volume averaging of mass, momentum equations.....	265
SOFT: a framework for semantic interoperability of scientific software	273
 POPULATION BALANCE	 279
Combined multifluid-population balance method for polydisperse multiphase flows	281
A multifluid-PBE model for a slurry bubble column with bubble size dependent velocity, weight fractions and temperature.....	285
CFD simulation of the droplet size distribution of liquid-liquid emulsions in stirred tank reactors	295
Towards a CFD model for boiling flows: validation of QMOM predictions with TOPFLOW experiments	301
Numerical simulations of turbulent liquid-liquid dispersions with quadrature-based moment methods.....	309
Simulation of dispersion of immiscible fluids in a turbulent couette flow	317
Simulation of gas-liquid flows in separators - a Lagrangian approach.....	325
CFD modelling to predict mass transfer in pulsed sieve plate extraction columns	335
 BREAKUP & COALESCENCE	 343
Experimental and numerical study on single droplet breakage in turbulent flow	345
Improved collision modelling for liquid metal droplets in a copper slag cleaning process	355
Modelling of bubble dynamics in slag during its hot stage engineering.....	365
Controlled coalescence with local front reconstruction method	373
 BUBBLY FLOWS	 381
Modelling of fluid dynamics, mass transfer and chemical reaction in bubbly flows	383
Stochastic DSMC model for large scale dense bubbly flows.....	391
On the surfacing mechanism of bubble plumes from subsea gas release.....	399
Bubble generated turbulence in two fluid simulation of bubbly flow	405
 HEAT TRANSFER	 413
CFD-simulation of boiling in a heated pipe including flow pattern transitions using a multi-field concept	415
The pear-shaped fate of an ice melting front	423
Flow dynamics studies for flexible operation of continuous casters (flow flex cc).....	431
An Euler-Euler model for gas-liquid flows in a coil wound heat exchanger.....	441
 NON-NEWTONIAN FLOWS.....	 449
Viscoelastic flow simulations in disordered porous media	451
Tire rubber extrudate swell simulation and verification with experiments	459
Front-tracking simulations of bubbles rising in non-Newtonian fluids.....	469
A 2D sediment bed morphodynamics model for turbulent, non-Newtonian, particle-loaded flows.....	479

METALLURGICAL APPLICATIONS.....	491
Experimental modelling of metallurgical processes	493
State of the art: macroscopic modelling approaches for the description of multiphysics phenomena within the electroslag remelting process	499
LES-VOF simulation of turbulent interfacial flow in the continuous casting mold	507
CFD-DEM modelling of blast furnace tapping	515
Multiphase flow modelling of furnace tapholes	521
Numerical predictions of the shape and size of the raceway zone in a blast furnace.....	531
Modelling and measurements in the aluminium industry - Where are the obstacles?	541
Modelling of chemical reactions in metallurgical processes.....	549
Using CFD analysis to optimise top submerged lance furnace geometries	555
Numerical analysis of the temperature distribution in a martensic stainless steel strip during hardening.....	565
Validation of a rapid slag viscosity measurement by CFD.....	575
Solidification modeling with user defined function in ANSYS Fluent.....	583
Cleaning of polycyclic aromatic hydrocarbons (PAH) obtained from ferroalloys plant.....	587
Granular flow described by fictitious fluids: a suitable methodology for process simulations	593
A multiscale numerical approach of the dripping slag in the coke bed zone of a pilot scale Si-Mn furnace.....	599
 INDUSTRIAL APPLICATIONS	 605
Use of CFD as a design tool for a phosphoric acid plant cooling pond	607
Numerical evaluation of co-firing solid recovered fuel with petroleum coke in a cement rotary kiln: Influence of fuel moisture	613
Experimental and CFD investigation of fractal distributor on a novel plate and frame ion-exchanger	621
 COMBUSTION	 631
CFD modeling of a commercial-size circle-draft biomass gasifier.....	633
Numerical study of coal particle gasification up to Reynolds numbers of 1000.....	641
Modelling combustion of pulverized coal and alternative carbon materials in the blast furnace raceway	647
Combustion chamber scaling for energy recovery from furnace process gas: waste to value	657
 PACKED BED.....	 665
Comparison of particle-resolved direct numerical simulation and 1D modelling of catalytic reactions in a packed bed	667
Numerical investigation of particle types influence on packed bed adsorber behaviour	675
CFD based study of dense medium drum separation processes	683
A multi-domain 1D particle-reactor model for packed bed reactor applications.....	689
 SPECIES TRANSPORT & INTERFACES	 699
Modelling and numerical simulation of surface active species transport - reaction in welding processes	701
Multiscale approach to fully resolved boundary layers using adaptive grids.....	709
Implementation, demonstration and validation of a user-defined wall function for direct precipitation fouling in Ansys Fluent.....	717

FREE SURFACE FLOW & WAVES	727
Unresolved CFD-DEM in environmental engineering: submarine slope stability and other applications.....	729
Influence of the upstream cylinder and wave breaking point on the breaking wave forces on the downstream cylinder	735
Recent developments for the computation of the necessary submergence of pump intakes with free surfaces	743
Parallel multiphase flow software for solving the Navier-Stokes equations	752
 PARTICLE METHODS	 759
A numerical approach to model aggregate restructuring in shear flow using DEM in Lattice-Boltzmann simulations	761
Adaptive coarse-graining for large-scale DEM simulations.....	773
Novel efficient hybrid-DEM collision integration scheme.....	779
Implementing the kinetic theory of granular flows into the Lagrangian dense discrete phase model.....	785
Importance of the different fluid forces on particle dispersion in fluid phase resonance mixers	791
Large scale modelling of bubble formation and growth in a supersaturated liquid.....	798
 FUNDAMENTAL FLUID DYNAMICS	 807
Flow past a yawed cylinder of finite length using a fictitious domain method	809
A numerical evaluation of the effect of the electro-magnetic force on bubble flow in aluminium smelting process.....	819
A DNS study of droplet spreading and penetration on a porous medium.....	825
From linear to nonlinear: Transient growth in confined magnetohydrodynamic flows.....	831

CFD MODELING OF DYNAMIC EMULSION STABILITY

A.V. Patil¹, S. T. Johansen¹

¹ SINTEF Materials and Chemistry, 7465 Trondheim, NORWAY

* E-mail: amit.patil@sintef.no

ABSTRACT

Assuring transport and separation of oil and water crude emulsions is of significant importance to the oil and gas industries. The crude oil, due to its profuse chemical composition, has complex dispersion and emulsion flow behavior with water. As a result, of the interface chemistry, the bubbles and droplets may separate easily, or not separate at all, impacting flow regime, water holdup, pressure drop and separation efficiency during pipe transport. Using a recently developed new stirred tank characterization technique for emulsion stability droplet relaxation parameters can be studied. Multiple model oils and crude oils were characterized by this technique. This work discusses development of a pragmatic modeling method that can validate the experimental measurements. A time averaged velocity profile in a stirred tank is used to obtain a 1-D flux flow profile in the vertical direction. This 1-D flux profile is used as a simplified flow equation and scalar equations for droplet size and dispersed phase fraction is used for modeling the emulsion stability and relaxation. This method can help in fast simulation of emulsion stability that involves long time scales of coalescence and breakage evolution for crude oil and water.

Keywords: Multiphase flow, oil-water emulsion, flow assurance.

NOMENCLATURE

A complete list of symbols used, with dimensions, is required.

Greek Symbols

- ρ Mass density, [kg/m³].
- μ Dynamic viscosity, [kg/m.s].
- Γ Dispersed phase viscosity, [m²/s].
- Ω relaxation coefficient, [1/s].

Latin Symbols

- a Characteristic area, [m²].
- p Pressure, [Pa].
- \mathbf{u} Velocity, [m/s].

\bar{U} Averaged velocity, [m/s].

\bar{d} mean droplet size, [m].

α dispersed phase fraction, [-].

\bar{V} Dispersed phase velocity, [m/s].

τ Relaxation time scale for droplets, [s].

Sub/superscripts

- c Continuous phase.
- A upward flow direction.
- B downward flow direction.
- E Exchange flow between A and B.
- z z- direction representing height direction of tank
- eq Equilibrium

INTRODUCTION

The pipeline transport of crude oil-water dispersions or emulsions is typical for many oil fields and flow assurance studies has been hampered by limited understanding of how to handle the possible behavior of the flow when stabilizing surfactants are present. The cost of crude oil production is strongly related to pressure drop produced in transport pipes. It is well known that pressure drop is strongly dependent on the rheological behavior, which is strongly influenced by emulsion stability. Therefore oil-water emulsion stability has been a subject to several studies in the past.

Emulsion stability or droplet size evolution is strongly influenced by interfacial tension (IFT) and surface chemistry (Aichele 2009; Mullins et. al. 2007; Sjoblom 2005). So there has been a need to quantify the droplet size evolution behaviour for given characteristics of oil-water emulsions. This has been achieved by an advanced imaging technique developed recently and presented in Patil et. al. (2017). In this method, the measurement of droplet size alongside torque provides the necessary understanding of dissipation on emulsion stability.

Experiments with model oils-water emulsion has shown that the droplet size in turbulent regimes is governed by Kolmogorov scale criteria (Kolmogorov, 1949). Depending on the regime defined by the inertial and viscous subrange; the equilibrium droplet size agree well with the theoretical correlations (Boxall et. al.

2010; Boxall et. al. 2012; Patil et. al. 2017). Further the dynamic droplet size relaxation of emulsions have also been studied by measuring the time dependent droplet relaxation and hence its coefficient (Calderbank, 1958; Patil et. al., 2017).

Dispersion of two phases by emulsification in a stirred tank has long been modeled using various multiphase modelling methods. Most common models for such fluid-fluid systems is the Euler-Euler method (Murthy et. al. 2007). Besides CFD methods using Population Balance models (PBM) to represent the dynamic dispersed phase have also been developed (Trætlie-Einarsrud et. al. 2014, Raikar et. al. 2009).

Generally for model oil-water emulsions the time scales for relaxations is several seconds (Patil et. al. 2017). For crude oil-water emulsions which have stabilizing components these time scales are higher (few minutes) (Patil et. al. 2017b). The challenges with using Euler-Euler methods (in 3D) is that they are slow and time consuming due to the small time steps needed ($<10^{-4}$ s). The CFD-PBM approach is still a useful modelling method. But a number of challenges were encountered in using such a method for emulsions where surface active components influence the droplet behavior.

For a normal stirred tank cell with a single impeller the radial and angular variation in dissipation is very small relative to the height. Therefore, a pragmatic 1-D model in height direction can make the model simplistic and fast. This will essentially also make emulsion stabilization modelling easy. Initially only the Sauter mean diameter (SMD) of the droplet will be modelled and later a size distribution model can be developed with a PBM kind of technique, like in Einarsrud et. al. (2014). In this work we describe the development of such a pragmatic 1-D model.

MODEL DESCRIPTION

The oil and water phase in the emulsion stability study are of nearly the same density and hence the 3-D flow patterns in the tank will not be much different from a single phase flow. So the flow pattern for the 3 speed levels of impeller can be evaluated using a single phase flow simulations. The properties of the continuous phase can be used for such a simulation.

The continuity and momentum equation for the 3D system is represented by;

$$\frac{\partial \rho_c}{\partial t} + \nabla \cdot (\rho_c \tilde{\mathbf{u}}_c) = 0 \quad (1)$$

$$\frac{\partial \rho_c \tilde{\mathbf{u}}_c}{\partial t} + \nabla \cdot \{ \rho_c \tilde{\mathbf{u}}_c \tilde{\mathbf{u}}_c \} + \{ \overline{\rho_c \mathbf{u}_c'' \mathbf{u}_c''} \} - \tau_c \} = -\nabla p + \rho_c g \quad (2)$$

Where, ρ_c is the density of continuous phase. Turbulent fluctuations are modelled with the k- ϵ model.

In these single phase simulations the impeller blade moments is integrated to obtain the torque. The torque is

monitored till equilibration is achieved. The simulation is continued further by time averaging the velocity field to obtain the averaged flux.

It is well known that the averaged velocity field for a baffled and flat blade impeller based stirred tank has a profile that looks like in Fig. 1. There are 2 circulation currents in the vertical z-direction. Both currents start at the impeller in radially outward direction. This results in a two large scale counter-rotating vortices. The upper vortex is moving up along the wall, above the impeller, while the lower vortex moving down along the wall, below the impeller. The flow recirculates back along the shaft as shown in Fig. 1. The upwards and downwards flow field sections is shown in Fig. 1 where the areas are marked. Within this flow pattern note that the upward and downward flow mass rate is always the same. The difference in the area is balanced by difference in mean velocities (z-directional).

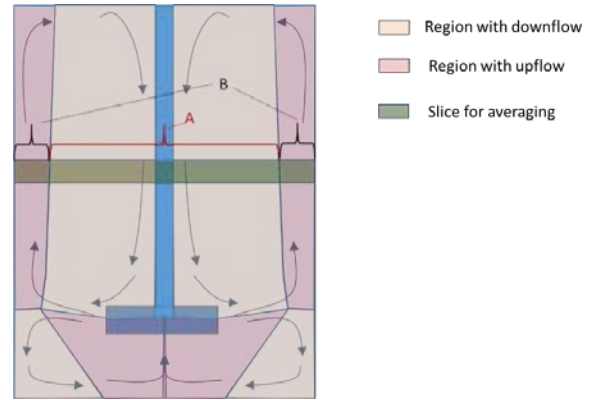


Figure 1: Regions with upward and downward flows are marked

This 3-D time averaged velocity field data is utilized to obtain a pseudo 1-D flow field in the vertical direction (z-direction) and horizontal directions. For this purpose, the flow fields in the cross section is averaged for upward and downward flow defined by region A and B at discrete cross sections along the z direction. Thus the upward and downward mean velocity and the upward and downward, and the corresponding cross sectional areas are evaluated. The averaged upward and downward velocity is given by;

$$\overline{U}_A = \frac{\int_A u_{c,z} da}{\int_A da} \quad \text{and} \quad \overline{U}_B = \frac{\int_B u_{c,z} da}{\int_B da} \quad (3)$$

Where, $u_{c,z}$ is the z-direction component velocity of the fluid velocity field $\tilde{\mathbf{u}}_c$. The flow area for the streams A and B are given by;

$$a_A = \int_A da \quad \text{and} \quad a_B = \int_B da \quad (4)$$

For evaluation of the average turbulent dissipation ϵ in horizontal slices, denoted A and B we define:

$$\overline{\varepsilon_A} = \frac{\int_A \varepsilon dV}{\int_A dV} \quad \text{and} \quad \overline{\varepsilon_B} = \frac{\int_B \varepsilon dV}{\int_B dV} \quad (5)$$

These dissipation rates, averaged over horizontal slices with finite thickness Δz , are critical input for evaluation of the equilibrium droplet sizes used by the model.

The mass conservation on a slice, for the zones A and B, is then given by:

$$\begin{aligned} [a_A \overline{U_A}]_z^+ - U_E a_I &= 0 \\ [a_B \overline{U_B}]_z^+ + U_E a_I &= 0 \end{aligned} \quad (6)$$

Here U_E is the average radially directed velocity (horizontal exchange velocity), communicating through area A_I , which is easily determined based on the interface location between zones A and B. The radial velocity U_E can be computed from any of the two relations in Eq.(6).

The above description for total flow balance is summarized in Fig. 2. It is to be noted that for each tank cross sectional area, the upward and downward volumetric flow is the same. This means that;

$$\overline{U_{A,k+\frac{1}{2}} a_{A,k+\frac{1}{2}}} = \overline{U_{B,k+\frac{1}{2}} a_{B,k+\frac{1}{2}}} \quad (7)$$

This is consistent with the global mass conservation equations, Eq. (6)

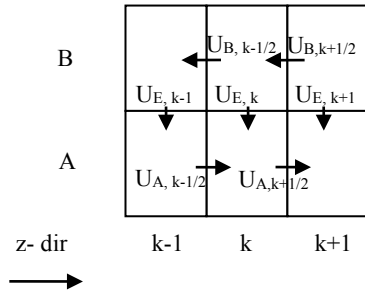


Figure 2: Grid description for the 1-D model

This 1-D averaged data is utilized in the dynamic droplet size model equation provided by;

$$\begin{aligned} \frac{\partial}{\partial t} a_A \overline{d_{A,z}} + \frac{\partial}{\partial z} (a_A V_z \overline{d_{A,z}}) &= \frac{\partial}{\partial z} \Gamma a_A \frac{\partial \overline{d_{A,z}}}{\partial z} \\ + a_A \frac{\overline{d_{eq,A,z}} - \overline{d_{A,z}}}{\tau} + \Omega a_I (\overline{d_{B,z}} - \overline{d_{A,z}}) & \quad (8) \\ + \frac{a_I}{\Delta z} (\max(U_E, 0) \overline{d_{B,z}} - \max(-U_E, 0) \overline{d_{A,z}}) & \end{aligned}$$

The above equation formulation is a passive scalar transport equation with source terms. The 3-D version of this can be found in Laux and Johansen (1999). Similarly for the droplet size in zone B:

$$\begin{aligned} \frac{\partial}{\partial t} a_B \overline{d_{B,z}} + \frac{\partial}{\partial z} (a_B V_z \overline{d_{B,z}}) &= \frac{\partial}{\partial z} \Gamma a_B \frac{\partial \overline{d_{B,z}}}{\partial z} \\ + a_B \frac{\overline{d_{eq,B,z}} - \overline{d_{B,z}}}{\tau} - \Omega a_I (\overline{d_{B,z}} - \overline{d_{A,z}}) & \quad (9) \\ - \frac{a_I}{\Delta z} (\max(U_E, 0) \overline{d_{B,z}} - \max(-U_E, 0) \overline{d_{A,z}}) & \end{aligned}$$

Where; $\overline{d_{A,z}}$ is the averaged droplet size in the zone of upward flow at position z . The above 1-D model is further simplified by neglecting the shear term defined by the viscosity of the continuous phase. Since this model is not taking the detailed flow into consideration the shear effect can be essentially lumped into Equilibrium droplet size $\overline{d_{eq,A,z}}$. The $\overline{d_{eq,A,z}}$ is a function of multiple factors defined by fluid properties and the presence of surface-active components. If the surface-active components are not present then depending on the flow regime the droplet size is governed by inertial or viscous sub-range correlations in (Patil et. al. 2017).

In these two equations ((8),(9)) Ω is a dispersion transfer coefficient, expressing the turbulence induced exchange rate of particle size between the two zones. The last term in Eqs. (8) and (9) express the convective transport between zones A and B.

The droplet fraction in zone A is conserved by:

$$\begin{aligned} \frac{\partial}{\partial t} a_A \overline{\alpha_{A,z}} + \frac{\partial}{\partial z} (a_A V_z \overline{\alpha_{A,z}}) &= \frac{\partial}{\partial z} \Gamma a_A \frac{\partial \overline{\alpha_{A,z}}}{\partial z} \\ + \Omega a_I (\overline{\alpha_{B,z}} - \overline{\alpha_{A,z}}) & \quad (10) \\ + \frac{a_I}{\Delta z} (\max(U_E, 0) \overline{\alpha_{B,z}} - \max(U_E, 0) \overline{\alpha_{A,z}}) & \end{aligned}$$

The above equation is a general mass conservation equation for dispersed phase assuming phase densities are constant. It is averaged over all the control volumes in the system. Similarly for zone B, we have

$$\begin{aligned} \frac{\partial}{\partial t} a_B \overline{\alpha_{B,z}} + \frac{\partial}{\partial z} (a_B V_z \overline{\alpha_{B,z}}) &= \frac{\partial}{\partial z} \Gamma a_B \frac{\partial \overline{\alpha_{B,z}}}{\partial z} \\ + \Omega a_I (\overline{\alpha_{B,z}} - \overline{\alpha_{A,z}}) & \quad (11) \\ - \frac{a_I}{\Delta z} (\max(U_E, 0) \overline{\alpha_{B,z}} - \max(U_E, 0) \overline{\alpha_{A,z}}) & \end{aligned}$$

The dispersed phase velocity in z -direction V_z has essentially two components, which are convective velocity U_z and terminal velocity.

$$V_z = U_z + V_t \quad (12)$$

Here V_t is the dispersed phase velocity component from Stokes law given by;

$$V_t = \frac{(\rho_c - \rho_d) d^2 g}{18\mu} \quad (13)$$

Further discretization and rearranging Eq. (8) gives the following equation to solve the (Sauter mean) droplet size equations in height direction.

$$\begin{aligned}
& \frac{a_{A,k}}{\Delta t} (\overline{d_{A,k,n+1}} - \overline{d_{A,k,n}}) + \frac{1}{\Delta z} \left[a_{A,k} (\overline{U_A} + \overline{V_t}) \overline{d_{A,k,z}} \right]_{z^-}^+ = \\
& \frac{1}{\Delta z} \left[\Gamma a_{A,k} \frac{\partial \overline{d_{A,k,z}}}{\partial z} \right]_{z^-}^+ \\
& + a_{A,k} \frac{\overline{d_{eq,A,k,z}} - \overline{d_{A,k,z}}}{\tau} + \Omega a_{I,k} (\overline{d_{B,k,z}} - \overline{d_{A,k,z}}) \\
& + \frac{a_{I,k}}{\Delta z} (\max(U_{E,k}, 0) \overline{d_{B,k,z}} - \max(-U_{E,k}, 0) \overline{d_{A,k,z}})
\end{aligned} \quad (14)$$

In equations (15) and (16) the notation z^+ and z^- denotes the cell boundary positions for the slice where the droplet size is computer. The averaged velocities U_A and U_B are always computed at these cell boundaries (staggered grid arrangement).

Before proceeding, we subtract the product of droplet size and fluid mass conservation eq. (6), and rearrange.

$$\begin{aligned}
& \frac{a_{A,k}}{\Delta t} (\overline{d_{A,k,n+1}} - \overline{d_{A,k,n}}) + \frac{1}{\Delta z} (a_{A,k} \overline{U_{A,k}})^+ (\overline{d_{A,k,n}} - \overline{d_{A,k,n}}) \\
& - \frac{1}{\Delta z} (a_{A,k} \overline{U_{A,k}})^- (\overline{d_{A,k,n}} - \overline{d_{A,k,n}}) \\
& + \frac{1}{\Delta z} \left[(a_{A,k} \overline{V_t})^+ \overline{d_{A,k,n}} - (a_{A,k} \overline{V_t})^- \overline{d_{A,k,n}} \right] = \\
& \frac{1}{\Delta z} \left[\Gamma_k a_{A,k} \frac{\partial \overline{d_{A,k,n}}}{\partial z} \right]_{z^-}^+ + a_{A,k} \frac{\overline{d_{eq,A,k,n}} - \overline{d_{A,k,n}}}{\tau} \\
& + \Omega_k a_{I,k} (\overline{d_{B,k,n}} - \overline{d_{A,k,n}}) \\
& + \frac{a_{I,k}}{\Delta z} (\max(U_{E,k}, 0) (\overline{d_{B,k,n}} - \overline{d_{A,k,n}}))
\end{aligned} \quad (15)$$

The values at the cell faces ($\overline{d_{A,k,z}^+}$ and $\overline{d_{A,k,z}^-}$) are now approximated by the upwind value, controlled by U_A or the terminal velocity V_t .

Note that here by convention, $\overline{U_{A,k}}$ and $\overline{U_{B,k}}$ are always positive representing the upward and downward velocity direction respectively. However, $\overline{V_t}$ and $\overline{U_E}$ can be positive or negative depending on density difference and direction of the flow respectively. If continuous phase density is larger than dispersed phase $\overline{V_t}$ is positive (in z direction). Else it is negative when dispersed has higher density.

At any given cross sectional grid say 'k' in z direction, if the exchange of mass is from B zone (downward flow) to A zone (upward flow) then the $\overline{U_{E,k}}$ is positive.

Similarly, vis-versa it is negative.

$$\begin{aligned}
& \frac{a_{A,k}}{\Delta t} (\overline{d_{A,k,n+1}} - \overline{d_{A,k,n}}) - \frac{1}{\Delta z} (a_{A,k} \overline{U_{A,k}})^- (\overline{d_{A,k,n}} - \overline{d_{A,k,n}}) \\
& + \frac{1}{\Delta z} \left[(a_{A,k} \overline{V_t})^+ \overline{d_{A,k,n}} - (a_{A,k} \overline{V_t})^- \overline{d_{A,k,n}} \right] = \\
& \frac{1}{\Delta z} \left[\Gamma_k a_{A,k} \frac{\partial \overline{d_{A,k,n}}}{\partial z} \right]_{z^-}^+ + a_{A,k} \frac{\overline{d_{eq,A,k,n}} - \overline{d_{A,k,n}}}{\tau} \\
& + \Omega_k a_{I,k} (\overline{d_{B,k,n}} - \overline{d_{A,k,n}}) \\
& + \frac{a_{I,k}}{\Delta z} (\max(U_{E,k}, 0) (\overline{d_{B,k,n}} - \overline{d_{A,k,n}}))
\end{aligned} \quad (16)$$

Similarly, a formulation for the downward flow droplet size equation exists given by;

$$\begin{aligned}
& \frac{a_{B,k}}{\Delta t} (\overline{d_{B,k,n+1}} - \overline{d_{B,k,n}}) + \frac{1}{\Delta z} (a_{B,k} \overline{U_{B,k}})^+ (\overline{d_{B,k,n}} - \overline{d_{B,k,n}}) \\
& + \frac{1}{\Delta z} \left[(a_{B,k} \overline{V_t})^+ \overline{d_{A,k,n}} - (a_{B,k} \overline{V_t})^- \overline{d_{A,k,n}} \right] = \\
& \frac{1}{\Delta z} \left[\Gamma_k a_{B,k} \frac{\partial \overline{d_{B,k,n}}}{\partial z} \right]_{z^-}^+ + a_{B,k} \frac{\overline{d_{eq,A,k,n}} - \overline{d_{A,k,n}}}{\tau} \\
& - \Omega_k a_{I,k} (\overline{d_{B,k,n}} - \overline{d_{A,k,n}}) \\
& - \frac{a_{I,k}}{\Delta z} (\max(U_{E,k}, 0) (\overline{d_{B,k,n}} - \overline{d_{A,k,n}}))
\end{aligned} \quad (17)$$

The conservation equations for the dispersed phase is given by eqs. (10) and (11). These equations as well, may be discretised, using explicit time integration and first order unwinding for convection.

It should be noted that the vertical dispersion coefficient Γ as well as the horizontal exchange coefficient Ω has not been determined yet. These may be estimated based on the mixing length hypothesis, or may be extracted from the CFD simulations. As a first approach we may neglect the effects of turbulent dispersion and convective dispersion will dominate in most cases.

Both the terminal velocity and the equilibrium size may be made explicitly depending on the droplet fractions. Accordingly, the terminal velocity V_t in equations (16) and (17), will depend on the solution of the droplet fraction equations (10) and (11).

For the top and bottom slices the boundary condition is that there is no flux of droplet size or droplet mass (volume fraction) across these external boundaries. The droplet fraction may build to large values in the end-of-domain cells. In this case over compaction may, as an example, be avoided by enforcing the droplet velocities to become stagnant at a maximum packing.

The 3-D single phase flow simulations of stirred tank was performed using ANSYS Fluent 17.1. The 3-D time averaged velocity field data was imported in MATLAB to obtain time averaged 1-D volumetric flow rate in height direction.

RESULTS

The averaged velocity vector plot for the 3-D flow field is shown hereby in Fig. 3 for a 3500 RPM impeller speed. This plot illustrates the flow field description provided earlier in the previous section Fig. 1.

The z-direction velocity field is shown in Fig. 4. Note that close to the impeller tip the fluid velocities are very high. Therefore, the scale in this fig has been limited to +1.5 and -1.5 m/s velocity range so that remaining flow features are better visible.

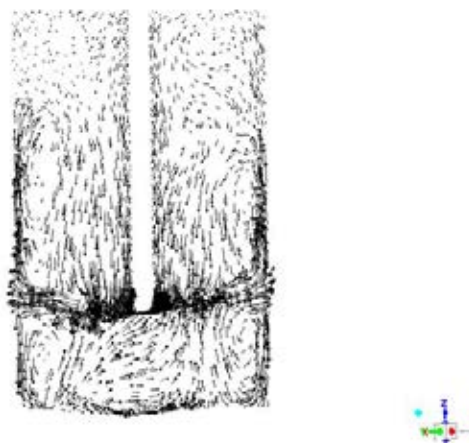


Figure 3: Cross sectional cut view of velocity vector field

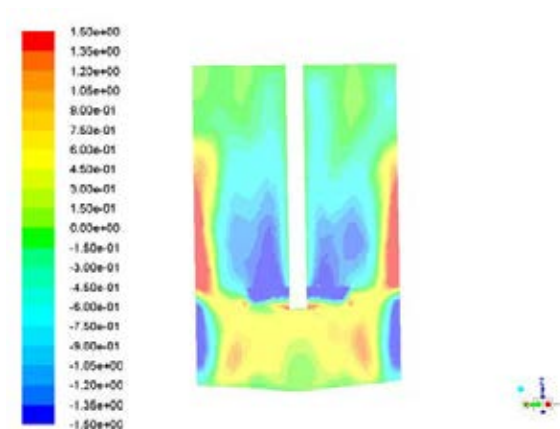


Figure 4: Cross sectional cut view of z-directional velocity colour profile

The data from the time averaging done over a 3-D simulation data for 25 s gave a profile that equilibrated and changed negligibly with time. Using this profile data the positive and negative averaged velocity fields were averaged at discrete cell faces in z direction. These cell face velocities are weighted with respect to cell face area as per Eq. (3) to give averaged upward and downward velocities.

Besides, integrating the upward and downward flow area provides averaged area of A and B. The volumetric flow rate in upward and downward direction can thus be obtained which both should be equal from Eq. (7).

Further using Eq. (6) the exchange velocity and volumetric flow rate between the two zones (A and B) can be obtained. The dimensions of the tank is summarized in Table 1.

Table 1: Model dimension.

Dimensions	
Tank diameter	0.095 m
Tank height	0.148 m
Impeller diameter	0.05 m
Number of cells in z direction	10
Grid size (z-direction)	0.0148 m

It is to be noted that though the averaging takes place for a long enough time there is always some small difference between the upward and downward flow

rates. Though this numerical difference is negligibly small they need to be removed for the 1-D simulation as this may cause numerical leakages for the dispersed phase equation.

Therefore, the upward and downward volumetric flow rate are averaged out as a reasonable approximation. Fig. 5 shows a plot of the averaged upward and downward volumetric flow rate for the 3-D simulation at 3500 RPM impeller speed. These are at cell face positions. Besides, it also shows a plot of cell exchange flow rate between A and B zone at cell centre position.

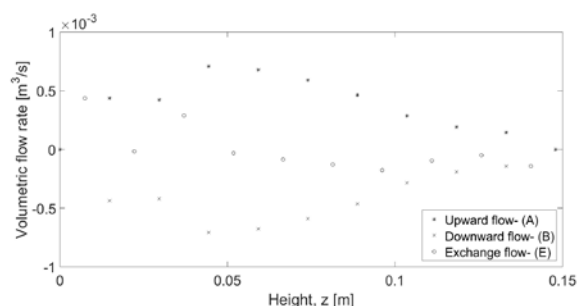


Figure 5: Upward and downward volumetric flow rate and exchange flow rate

This has provided a complete internally balanced velocity field that can be used for dispersed phase simulations. Using such a 1-D method, fast simulation of dispersed phase evolution is possible. With this method, the long time scales of emulsion droplet size relaxation can be modelled.

CONCLUSION

A simplified 1-D modelling method has been proposed to mimic emulsion stability in stirred tank. This method uses time averaged velocity fields from 3-D single phase simulations to obtain 1-D flow rate in z direction (upward and downward direction). This balanced flow rate field can be further used for modelling the size evolution of a dispersed phase in the height or z direction. Using such a method long time scales of emulsion evolution can be modelled fast. These models can be fitted with emulsion evolution parameters obtained experimentally using a stirred tank. Such models can in future be used in 1-D pipe simulation software.

REFERENCES

- AICHELE, C., (2009), "Characterizing Water-in-oil Emulsions with Application to Gas Hydrate Formation", *PhD thesis, Rice University*, 2009.
- MULLINS O., SHEU E., HAMMAMI A., MARSHALL A., (2007), "Asphaltenes, Heavy Oils, and Petroleomics", *Springer New York*.
- J. SJOBLM, (2005), "Emulsions and Emulsion Stability: Surfactant Science Series/61", *Surfactant Science, CRC Press*.
- PATIL A.V., MARTI X.S., TETLIE P., JOHANSEN S.T., "Development of an advanced imaging technique

for dynamic emulsion stability”, accepted by *Chem. Engg. J.*

KOLMOGOROV, A., (1949), “On the disintegration of drops in a turbulent flow”, *Dok. Akad. Nauk.*, **66**, 825-828.

BOXALL J. A., KOH C. A., SLOAN E. D., SUM A. K., and WU D. T., (2010), “Measurement and calibration of droplet size distributions in water-in-Oil emulsions by particle video microscope and a focused beam reflectance method”, *Ind. and Engg. Chem. Res.*, **49**, 1412-1418.

BOXALL, J. A., KOH, C. A., SLOAN, E. D., SUM, A. K., and WU, D. T., (2012), “Droplet size scaling of water-in-oil emulsions under turbulent flow”, *Langmuir: The ACS Journal of Surfaces and Colloids*, **28**, 104-110.

CALDERBANK P., (1958), “Physical rate processes in industrial fermentation. Part i; the interfacial area in gas-liquid contacting with mechanical agitation”, *Trans. Instn. Chem. Eng.* 36 443-463.

MURTHY B.N., GHADGE R.S., JOSHI J.B., (2007), “CFD simulations of gas-liquid-solid stirred reactor: Prediction of critical impeller speed for solid suspension”, *Chem. Engg. Sci.*, **62**, 7148-7195.

TRÆTTLI-EINARSRUD K. E., PANJWANI B., PAUCHARD V., (2014), “A pragmatic approach to CFD modelling of separation processes”, *Proceedings of 10th International Conference on CFD in Oil & Gas, Metallurgical and Process Industries, Trondheim, Norway, June 2014.*

RAIKAR N. B., BHATIA S. R., MALONE M. F., HENSON M. A., (2009), “Experimental studies and population balance equation models for breakage prediction of emulsion drop size distributions”, *Chem. Engg. Sci.*, **64(10)**, 2433-2447.

LAUX H., and JOHANSEN S.T., (1999), “A CFD analysis of the air entrainment rate due to a plunging steel jet combining mathematical models for dispersed and separated multiphase flows”, *Fluid Flow Phenomena in Metal Processing, Edited by N. El-Kaddah et al., The Minerals, Metals and Materials Society*, 21-30.